Strategos, 5(2), 2021, 109-133
UDK 32
UDK 355/359
Professional papers[1]

STRATEGOS

Application of Sentinel-1 SAR Imagery for Flood Detection and Monitoring, Case Study of Floods in Vrgorac Region during November and December 2020

Mladen Viher

Abstract

The paper presents digital image processing methods that, applied sequentially, enable detection and monitoring of flooded areas using satellite images obtained by Synthetic Aperture Radar (SAR) from Sentinel-1 satellite in the case study of floods in the Vrgorac region, during November and December 2020. The method is based on the scattering of a polarized radar wave on water surfaces. The paper comments on the advantages and disadvantages of using open resources and proposes the urgent accession of the Republic of Croatia to the Charter on Space.

Key words

natural disasters, floods, GEOINT, SAR, Sentinel-1, remote sensing

1 The article was received by the Editorial Board on October 18th, 2021.accepted for publication on December 6th, 2021.

Introduction

The topic of this paper is the possibility of detecting and monitoring a flooded area using satellite radar images to detect and map flooded areas. The flood in the area of the town of Vrgorac was caused by an extreme amount of precipitation, with a daily amount of up to 80 mm per square meter, which caused the flourishing of karst watercourses, and lasted from November 29 to December 21, 2020 and was declared a natural disaster. The floods affected agricultural areas in the lowlands, and the village of Kokorići suffered the most severe damage, where water penetrated houses and caused great damage. A thick layer of clouds and rain, which was accompanying this natural disaster, made it impossible for other sensors to operate. The imaging radar image provides a quick insight into the size of the flooded area and the prioritization of the degree of endangerment of people and property and then the environment impact. At the same time, the imaging radar image provides an overview of available communications (e.g. the E65 motorway remained passable at all times) as well as areas for evacuation and setting up temporary settlements, warehouses and intervention forces depots.

Similar research has been conducted with other sensors, specifically by determining the so-called Normalized Difference Water Index (NDWI) using a radiometric multispectral sensor on the Sentinel-2 satellite (Župan et al., 2019a) where the main drawback is the unavailability of images during night and in cloudy conditions. In general, satellite radar sensors enable continuous recording of flooded areas, regardless of night and clouds, and are complementary to radiometric images in periods favourable for the application of this type of sensor (Župan et al., 2019a; Župan et al. 2019c). Sentinel-1 is the first radar satellite pair in the European Copernicus program initiated at the turn of the century by the European Commission in collaboration with the European Space Agency. Sentinel-1A was launched on April 3, 2014, followed by the identical Sentinel-1B satellite launched on April 25, 2016. Their primary sensor is a Synthetic Aperture Radar (SAR) operating in the C-band, at 5405 MHz with a radiometric accuracy of 1 dB in four different operating modes (Veci, 2016):

- Strip Map (SM)

- Interferometric Wide Swath (IW)
- Extra Wide Swath (EW) and
- Wave (WV).

SM mode allows a maximum spatial resolution of 5x5 meters in the 80 km wide coverage band in single (horizontal HH, vertical VV) or double polarization (HH + HV, VV + VH). SM mode allows continuity with earlier satellite missions: ERS and Envisat. The sensor does not work continuously in this mode, so images are not always available. This mode is intended for crisis situations and imaging of small islands and it is necessary to require remote sensing of the desired area.

IW mode has a longer range, 250 km, with lower resolution perpendicular to the projection of the satellite's trajectory on the ground; 5x20 m, in single or double polarization, as in SM mode. At the same time, the radar beam moves in azimuth, thus allowing better resolution of the image of this image radar. This technique is called Terrain Observation with Progressive SAR (TOPSAR) and results in a scene consisting of three times nine sub-areas (so-called "swaths" and "bursts"). The difference between them is that "bursts" can be concatenated, while for "swaths" it is necessary to make separate products which can later be merged into a mosaic of satellite images. IW mode is used in radar interferometry (soil deformation after earthquakes, drifts, landslides,…), and it was also used in this paper, at the level of GRD (Ground Range Detected), which will be described in more detail below. This is the basic mode of Sentinel-1 sensor over land.

For ocean and polar regions, the EW mode is applicable where the SAR has 400 km long swath with resolution of 25x100 m, also in single or double polarization. The difference compared to the previous IW mode is that the EW has five swaths. EW mode is used for coastal and ocean areas, for monitoring marine pollution and for ice-cover conditions.

WV is a mode specialized for oceanographic needs in which the sensor creates clips of images measuring 20x20 km with pixels with a spatial resolution of 5x20 m. In this mode the radar does not work continuously and the distances between images are about 100 km.

ESA, as the operator of the Sentinel constellation, provides open access to satellite data through the Copernicus program, and satellite imagery is available within one hour for emergency (NRT; Near Real-Time – Emergency Response), within three hours at the special request of the operator, while all other users can access the images within 24 hours after the acquisition through the open hub of the Copernicus project, for which the Faculty of Geodesy of the University of Zagreb is "the relay" in the Republic of Croatia (URL http://science.geof.unizg.hr/copernicus/ , free service with prior registration of users). It is also possible to request priority recording in high resolution (https://emergency.copernicus.eu/mapping/ems/who-can-use-service) for which the Directorate of Civil Protection is authorized. An alternative is to use commercial satellites, such as COSMO SkyMed and Radarsat, whose imagery is valued up to several thousand euros. For example, the use of images from the COSMO SkyMed satellite, with a time resolution of 6 hours, in ScanSAR resolution of 30 x 30 m, during the observed period of natural disaster in the Vrgorac region, would amount to more than EUR 138,000 (e-GEOS, 2017).

Sentinel-1 recordings can be pre-processed at one of four levels:

- Level 0
- Level 1 SLC, Single Look Complex
- Level 1 GRD, Ground Range Detected
- Level 2 OCN, Ocean.

Level 0 is source, raw, SAR data that is compressed by the FDBAQ (Flexible Dynamic Block Adaptive Quantization) method and out of focus. Significant noise is present at this level and the recording is still uncalibrated. The satellite operator saves imagery at this source level in archives because pre-processed images are created from them.

Level 1 is appropriate for most users and has been used in this paper. Level 0 data undergo internal calibration and preprocessing and focusing (Miranda, 2015). At this level, preprocessing can result in preserved phase information in which case we obtain a satellite image with channels containing phase and signal amplitude in the form of complex numbers that can be further processed by standard mathematical methods developed in digital image

processing. This is the so-called Single Look Complex (SLC) which is applicable in interferometric processing of SAR images. In this paper, the methods for detecting flooded surfaces were based on the differences in the polarity of the transmitted and scattered radar beam, and GRD pretreatment was used, where the most accurate signal amplitude is cleared of noise by multiple observations of one and the same pixel. GRD images are projected onto the WGS84 ellipsoid and as such can be further merged into mosaics.

Level 2 Ocean (OCN) is used to determine wind waves and directions over the oceans and is not applicable in the detection and monitoring of flooded areas.

The Sentinel-1A and Sentinel-1B satellite pair with SAR sensors are fully suitable for detection and monitoring of flooded areas due to their technical characteristics (Tables 1 and 2). These are satellites that use proven satellite SAR technology, developed on satellites with SAR sensors of the previous generation: Seasat, ERS-1/2, JERS, SIR-C / X-SAR, Radarsat-1, SRTM, ENVISAT / ASAR, ALOS / PalSAR and complementary to current SAR missions: TerraSAR-X, Radarsat-2, COSMO SkyMed, RISAT, etc. Methods of acquisition and processing of SAR images are nowadays well developed, documented, and software and hardware supported. Taken together, this creates an enabling environment for the development of methods for detecting and monitoring floods in the context of the national GEOINT (geospatial intelligence discipline[2]) in support of military operations in cases of major natural and technical disasters (Viher et al., 2021), which is the topic of this paper.

2 GEOINT combines the capabilities of remote sensing, analysis of imagery and geospatial information, so that geographically referenced objects and activities on the Earth would be described, assessed and visually displayed.

Table 1. Technical and operational characteristics of the Sentinel-1 satellite (according to https://sentinels.copernicus.eu/web/sentinel/missions/sentinel-1)

Characteristics	Description
Manufacturer	Thales Alenia Space, Astrium Satellites, DLR i Jena-Optronik
Launch dates	Sentinel-1A 3rd April 2014 Sentinel-1B 25th April 2016 Rocket Soyuz, launch site Kourou, French Guiana
Expected mission duration	7 – 12 godina, planirana zamjena parom satelita Sentinel-1C i Sentinel-1D
Launch mass	2300 kg
Dimensions	3.9 x 2.6 x 2.5 m3
Orbit parameters	near polar, Sun synchronised 693 km altitude over WGS84 orbital period 98.6 minutes Repeat interval 12 days
Stabilization	all three axes
Downlink bandwidth	2 x 260 Mbps, X-band

Table 2. Technical characteristics of C-SAR sensors on Sentinel-1A and Sentinel-1B satellites (according to https://sentinels.copernicus.eu/web/sentinel/missions/sentinel-1)

Characteristics	Description
Centre frequency	5.405 GHz (C-band)
Pulse Repetition Frequency	1 – 3 kHz
Polarization	HH+HV, VV+VH, VV, HH
Bandwidth	0-100 MHz
Antenna size	12.3 m x 0.821 m
Azimuth beam width	0.23°
Elevation beam width	3.43°
Data quantization	10-bit

Applied methods

Considering the size of the GRD, which covers a much larger area than the flooded one, in the first step only the narrower area of interest was extracted, using a part of image which completely covers the flooded areas. Since Sentinel-1A and Sentinel-1B have identical orbits, separating the rectangular area is relatively simple. A rectangular area determined by the diagonal (43.227 ° N, 17.501 ° E) (43.148 ° N, 17.278 ° E) was selected and shown in Figure 2, which is not yet geocoded, and since the satellite was moving in a descending orbit equator, it shows the relative position of objects on the surface in its original form as collected by the sensor. Therefore, the relative relationship of the position of the place (e.g. Vrgorac and Kokorići) still does not correspond to their relative geographical position.

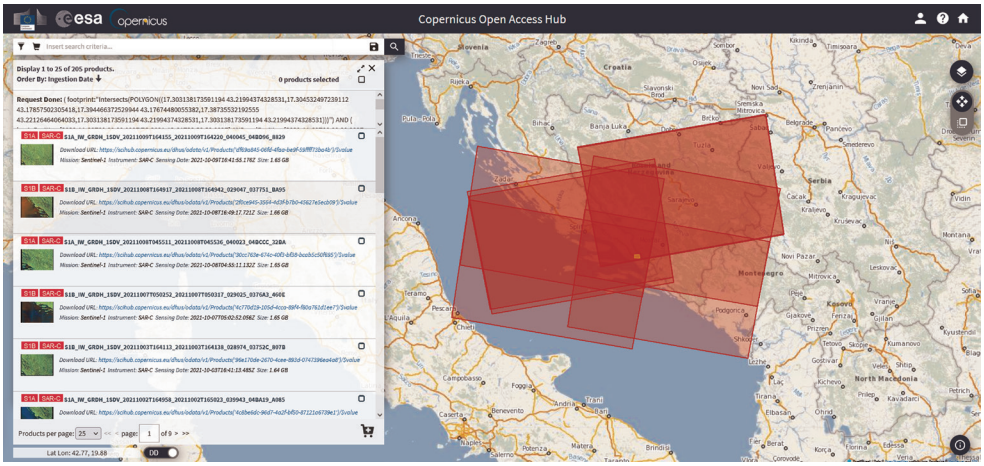

Figure 1. ESA OpenHUB – Available images of the Sentinel-1A and Sentinel-1B satellites at the Copernicus Open Hub covering the area affected by the flood in the area of the town of Vrgorac from November 29 to December 21, 2020.

Considering the size of the GRD, which covers a much larger area than the flooded one, in the first step only the narrower area of interest was extracted, using a part of image which completely covers the flooded areas. Since Sentinel-1A and Sentinel-1B have identical orbits, separating the rectangular

area is relatively simple. A rectangular area determined by the diagonal (43.227 ° N, 17.501 ° E) (43.148 ° N, 17.278 ° E) was selected and shown in Figure 2, which is not yet geocoded, and since the satellite was moving in a descending orbit equator, it shows the relative position of objects on the surface in its original form as collected by the sensor. Therefore, the relative relationship of the position of the place (e.g. Vrgorac and Kokorići) still does not correspond to their relative geographical position.

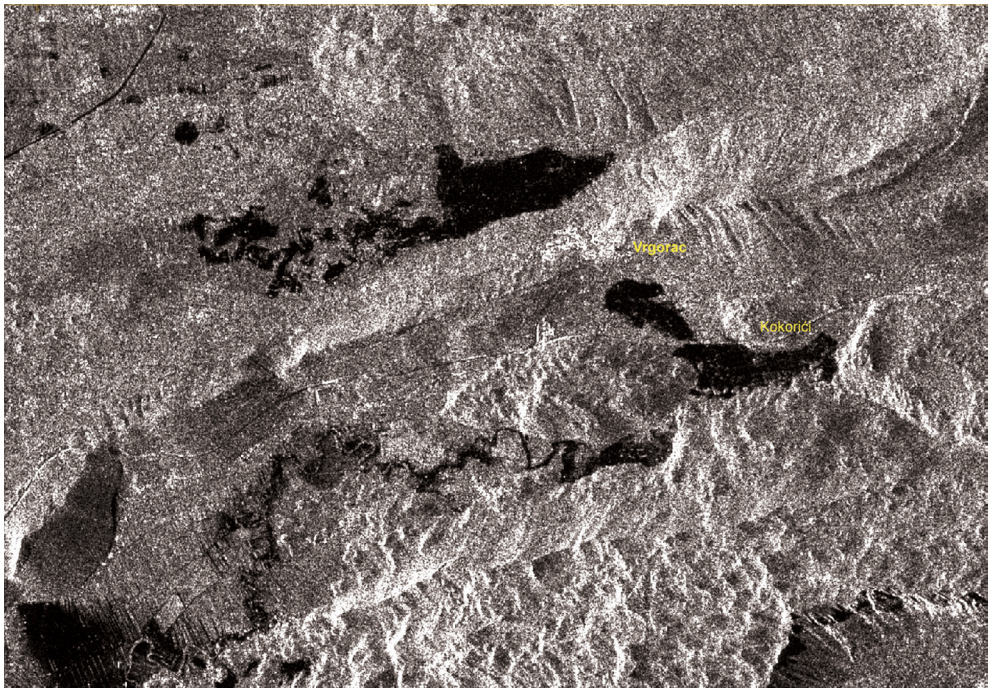

Figure 2. Subset – Selected area of interest that was threatened by floods near the town of Vrgorac in November and December 2020.

Polarization matrix

To detect flooded surfaces, a SAR sensor emits an electromagnetic wave whose electric field strength is on the transmitter, which is reflected from the surface and returned back to the sensor antenna (Anusha and Bharathi, 2019). In doing so, it twice crosses the distance r and returns to the antenna of the receiver, which then has the strength of the reflected electromagnetic wave.

This strength of the electric field of an electromagnetic wave, depending on the polarization of the transmitted and received wave described by the matrix S, can generally be expressed (Moriera et al., 2013):

$$\vec{E}_r = \frac{\exp(-jkr)}{r}\mathbf{S}\vec{E}_t^* \tag{1}$$

Where j is an imaginary unit, * denotes a conjugate complex vector, and k is the wave number for the wavelength of C-SAR on the Sentinel-1 satellite λ = 5.5465763 cm is:

$$k = \frac{2\pi}{5.5465763 \cdot 10^{-2}\,\mathrm{cm}} = 113.28043\,\mathrm{m}^{-1} \tag{2}$$

Equation (1) can be written out by components, H – horizontal polarization, V – vertical polarization, in order to study in detail the effect of polarization:

$$\begin{bmatrix} E_{r,H} \\ E_{r,V} \end{bmatrix} = \frac{\exp(-jkr)}{r} \cdot \begin{bmatrix} S_{HH} & S_{HV} \\ S_{VH} & S_{VV} \end{bmatrix} \cdot \begin{bmatrix} E_{t,H} \\ E_{t,V} \end{bmatrix}^* \tag{3}$$

In this way, through the polarization matrix S, the difference between scatterings is described:

HH – horizontally polarized on transmission, horizontally polarized on reception

VV – vertically polarized on transmission, vertically polarized on reception

HV – horizontally polarized on transmission, vertically polarized on reception

VH – vertically polarized on transmission, horizontally polarized on reception.

To detect water surfaces, we use the empirical fact that water surfaces are almost mirror reflectors, which means that their reflection will be weak because the reflected wave will go away from the receiver (Yamaguchi, 2020). This will result in low intensity, which is shown as dark areas in Figure 2. Despite the fact that we will detect water surfaces in VV polarization, expression (3) was not simplified. VH polarization was retained because it exists in GRD product. Both VV and VH polarizations are used for SAR composite on which, in various colours, a very complex scene of this karst terrain is easier to interpret.

Radiometric calibration σ^0

For comparability with other images of the same terrain, radiometric calibration was performed by squaring the digital value of the pixel (DN) in absolute terms and dividing by the square of the scattering coefficient σ^0 for the corresponding pixel (Moriera et al., 2013):

$$C_{ij} = \frac{\left|DN_{ij}\right|^2}{\left(\sigma_{ij}^0\right)^2} \tag{4}$$

Using the same polarization coefficients from (3)

$$\sigma_{ij}^0 = 4\pi \left|S_{ij} S_{ij}^*\right|. \tag{5}$$

The result is shown in Figure 3, which can now be directly compared to other images of the same sensor. Inherent noise should be removed from it in the next steps, and after all the radiometric enhancements we make,

we can geocode it and translate it into one of the standard projections for overlapping on GIS substrates.

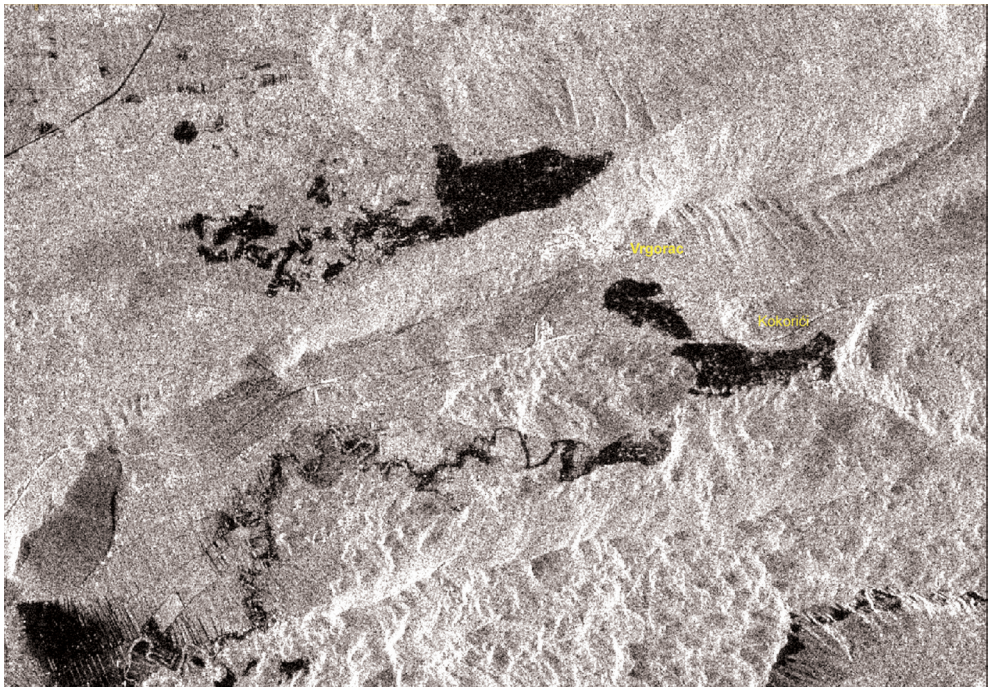

Figure 3. Radiometric calibration – Calibrated SAR image in VV polarization becomes directly comparable with images from the same sensor.

Inherent noise filtering

On the calibrated intermediate result (Figure 3) there is a significant inherent noise (so-called "salt-and-pepper"), which arises from the interference of the radar reflection inside and near the observed pixel, and manifests itself as a random spatial distribution of constructive and destructive interference. This type of noise can be removed:

- With a space filter
- With multiple recordings of the same surface (so-called multilook).

Filtering was performed with a space, Lee, filter. The Lee filter model is based on the fact that the image gives the pixel intensity C_{ij} which is proportional to the electric field strength in the reception, after the calibration performed in the previous step and which is the convolution of the actual pixel x_{ij} and random noise n_{ij} (Yamaguchi, 2020):

$$C_{ij} = x_{ij} \cdot n_{ij} . \tag{6}$$

Since *nij* is a random variable, different from pixel to pixel, there is no other way than statistical to estimate it, based on the arithmetic mean of the number of pixels within the square convolution kernel with the observed pixel in its middle. Convolution kernels can have 3x3, 5x5, 7x7,… pixels which is a matter of skill; there is no way to objectively determine which convolution kernel size is the most appropriate. Generally speaking, larger convolution kernels average the image better, but with the inevitable loss of sharpness. Images with lower noise can be filtered with smaller convolution kernels (3x3 and 5x5), while those with strong noise should be filtered with larger ones. In this paper, a 5x5 convolution kernel was used, which was determined empirically; first filtering with a 3x3 kernel was tested, followed by larger kernels, and the results were visually compared with respect to residual noise. The idea of the Lee filter is that we can estimate the value of pixel $\hat{C}_{ii}$ which is approximately the actual value of pixel xij:

$$\hat{C}_{ij} \approx x_{ij} \tag{7}$$

where we calculate the mean pixel value and estimate the variance around the centre pixel $\overline{x}_{ij,k}$ from the pixels covered by the convolution kernel of size *k* (e.g. 5x5 pixels), and for the estimated value of variance $\hat{\sigma}_{ij,k}$ in the case of C-SAR sensor on Sentinel-1A satellite, it is assumed $\hat{\sigma}_{ij,k}$ = 0.05 (Rubel et al., 2019):

$$\hat{C}_{ij} = \overline{x}_{ij,k} + \frac{\hat{\sigma}^2_{ij,k}}{\overline{x}_{ij}\sigma^2_{\mu} + \hat{\sigma}^2_{ij,k}} \left(x_{ij} - \overline{x}_{ij,k} \right) . \tag{8}$$

After the Lee filter application, we get an intermediate result with the inherent noise removed, with the inevitable loss of sharpness. The reason for this is that all filters that perform spatial averaging remove high-frequency phenomena, which can also be natural, for example edges or areas with a notable spatial variance change.

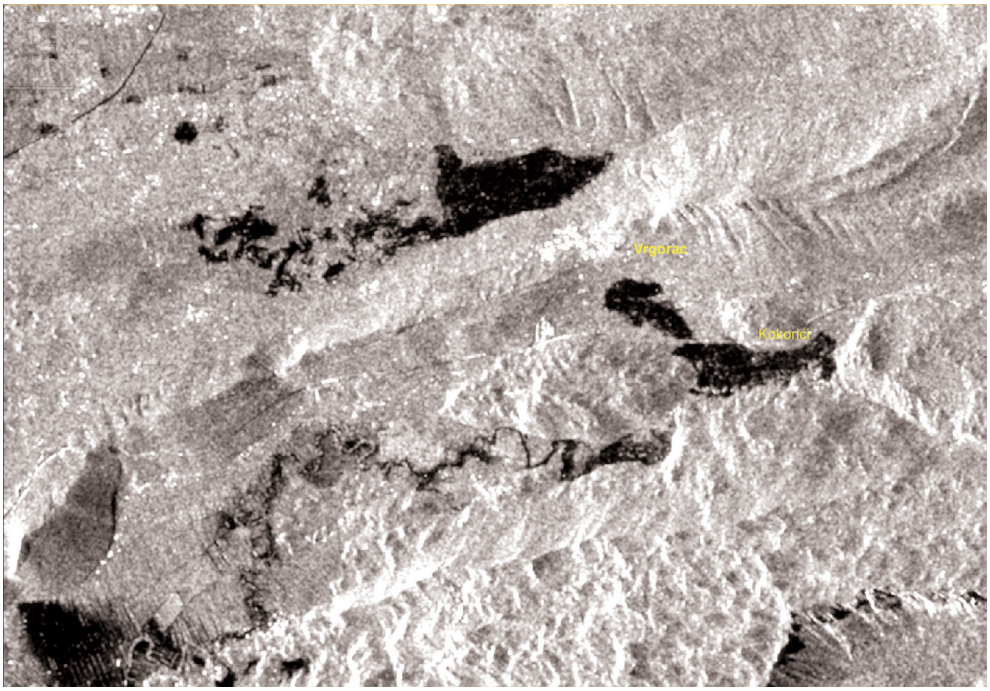

Figure 4. Inherent noise filtering – After processing the calibrated image (Figure 3), an image without inherent noise was obtained, but with slightly lower sharpness (see text), the image is still not geocoded and relative field positions are shown as seen by the sensor in the original image.

Geocoding

In this phase of processing, radiometric and geometric improvements of the image have been made, and its geocoding can be approached, whereby the pixels will get the relationships they have in reality, mapped to one of the

standard map projections. Image geocoding is an automated process, details of which will not be further discussed, since it is not the subject of this paper. It should be noted that we use data on the exact position of the satellite (which is stabilized on all three axes) and sensor orientation. For the geoid model, digital terrain models derived from the results of the Shuttle Radar Topography Mission (SRTM) with a resolution of 3 "x 3" or 1 "x 1" are used, depending on the application. The Copernicus portal offers the possibility of other digital terrain models, and in this paper SRTM resolution 1 "x 1" is used, which is a spatial resolution of about 30 meters at medium latitudes.

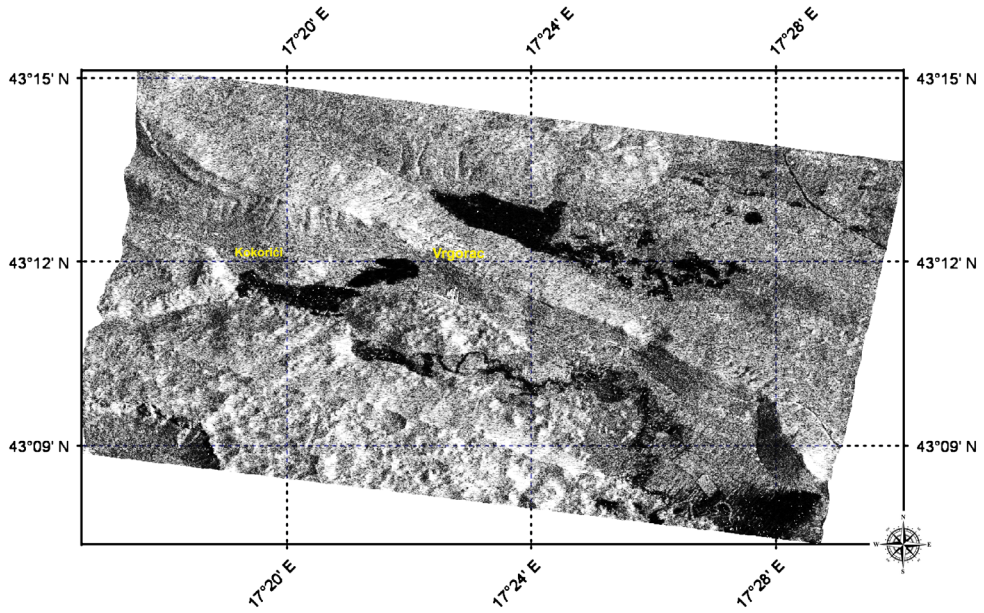

Figure 5. Geocoding – Geocoded image of the area around the town of Vrgorac, taken on 12.12.2020 around 04:50 local time from the C-SAR sensor on the Sentinel-1A satellite.

In the intermediate result, shown in Figure 5, water surfaces are presented as the darkest areas, where the pixel intensity is low. This is due to the reflection of the VV polarized wave which, according to expression (3), bounced off the water surface away from the radar sensor, which is why the radar receiver does not register a significant reflection.

Radar composite

For the visual interpretation of the radar image, we can also apply the VH component contained in the GRD, using three RGB channels (Anusha and Bharathi, 2019):

- Red for VV polarization
- Green for VH polarization and
- Blue for VV / VH ratio.

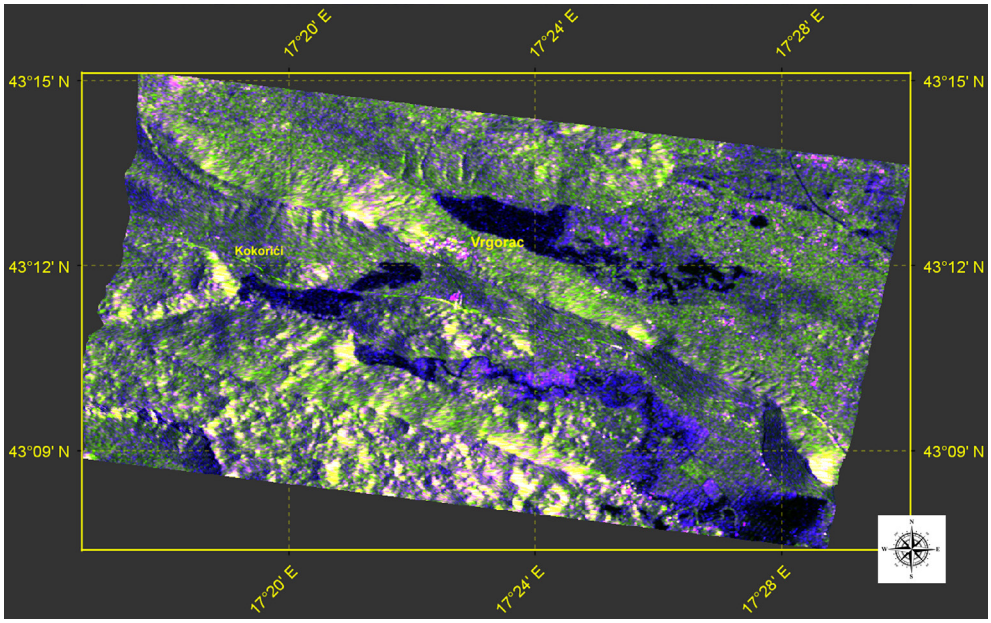

Figure 6. Three-channel composite – RGB composite obtained by different polarizations of the SAR image allows a more detailed subjective interpretation of the karst terrain scene; black are water surfaces, blue and dark purple are flat fields, green-yellow is karst terrain, and light purple are strong reflections from buildings in settlements (Mason et al., 2021).

In this way we will get a three-channel composite (Figure 6) in which radar smooth surfaces are shown as black areas (water surfaces), and those slightly less smooth as blue areas. Yellow and green are radar rough karst and wooded

surfaces, while settlements, with strong reflections from angular reflectors (e.g. buildings) are purple. This step does not have to be done, but since it is not a demanding classification of the image, it is quickly obtained and is useful in the next segmentation step in which, again almost empirically, water surfaces are separated (Mason et al., 2021).

Separation of water surfaces

The separation of water surfaces from Figure 5 is carried out on the basis of a histogram on which the bimodal distribution (two maxima, as in Figure 7) should be well observed if the area of interest has been cut out well. Too large areas of interest generally remain single-modal and then the VV polarization limit value is difficult to determine. In practice, this should not be a problem because water surfaces are immediately noticeable on the VV polarization.

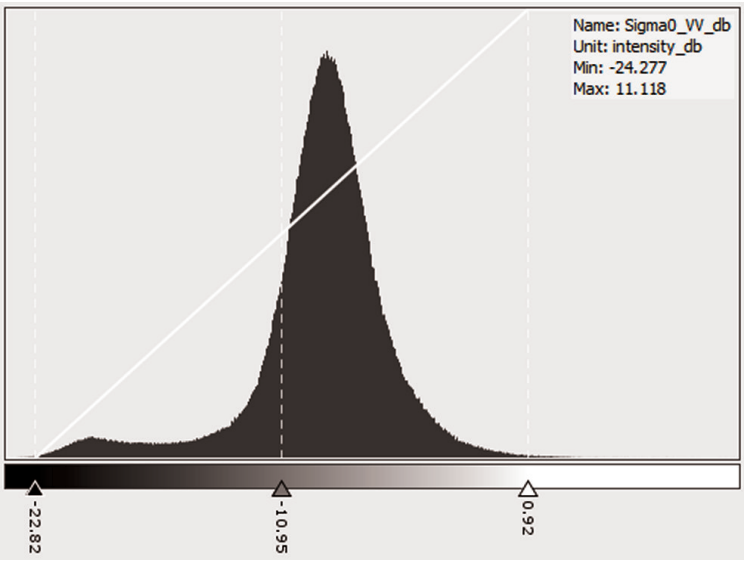

Figure 7. Bimodal intensity distribution – If we segment the display of the received signal strength to the range from -22.67 dB to -16.78 dB (Figure 8) we will include the left, less pronounced mode, which separates areas of weak VV reflection characteristic of water surfaces.

The histogram of the intermediate result shown in Figure 5 has exactly the desired bimodal distribution, with the left, less pronounced mode, belonging to the distribution of pixels from smooth, watery surfaces, from which the radar sensor received the weakest signal. To facilitate the interpretation of the large signal strength range, it has been translated into the decibel scale. From the area in Figure 5, the radar received signals in the range of -24,277 dB to 11.18 dB, but Figure 5 shows only those in the range of -22.82 dB to 0.92 dB, resulting in better image contrast, as they are extremely strong and extremely weak signals that rarely occurred.

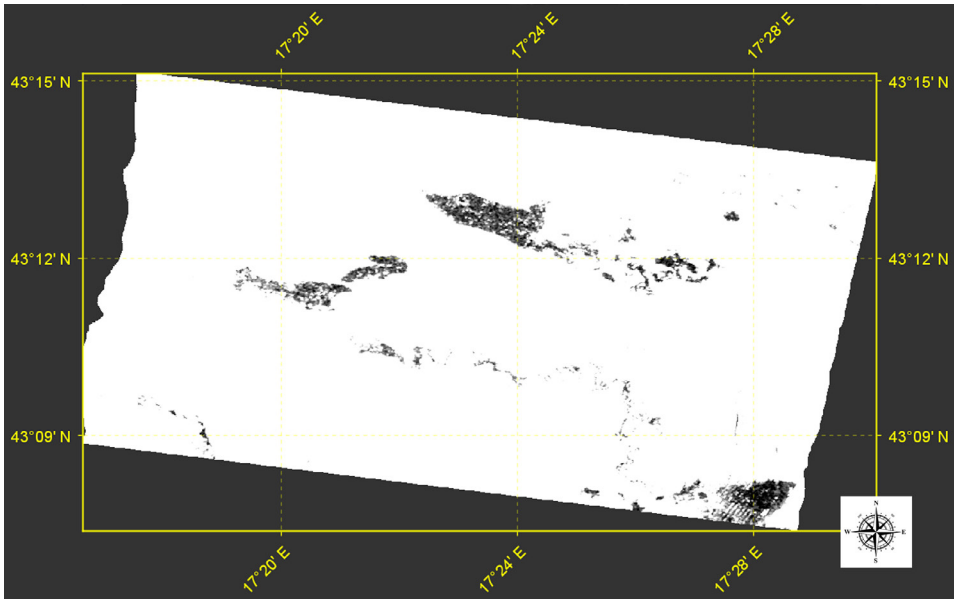

Figure 8. Segmentation - By segmenting the signal in the range from -22.67 dB to -16.78 dB, only the left, less pronounced mode of distribution of the VV signal strength was separated, thus separating the detected water surfaces.

The new intermediate result is a binary image of detected water surfaces and those that are not. All surfaces in the image that are not detected as water are converted to transparent and we get a raster layer with detected water surfaces that can be coloured as desired, e.g. blue. The next step is

not mandatory, but it contributes to the generalization of the representation of water surfaces, especially if vectorization of water surfaces is carried out (the original satellite image is raster). In this case a geometric low-pass filter can be applied, for example a median filter. The choice of filter and the size of the convolution kernel were determined empirically. In this paper, the median filter with a convolution kernel of 7 x 7 pixels proved to be good (small flooded areas were removed, as well as small dry areas within larger bodies of water, Figure 9).

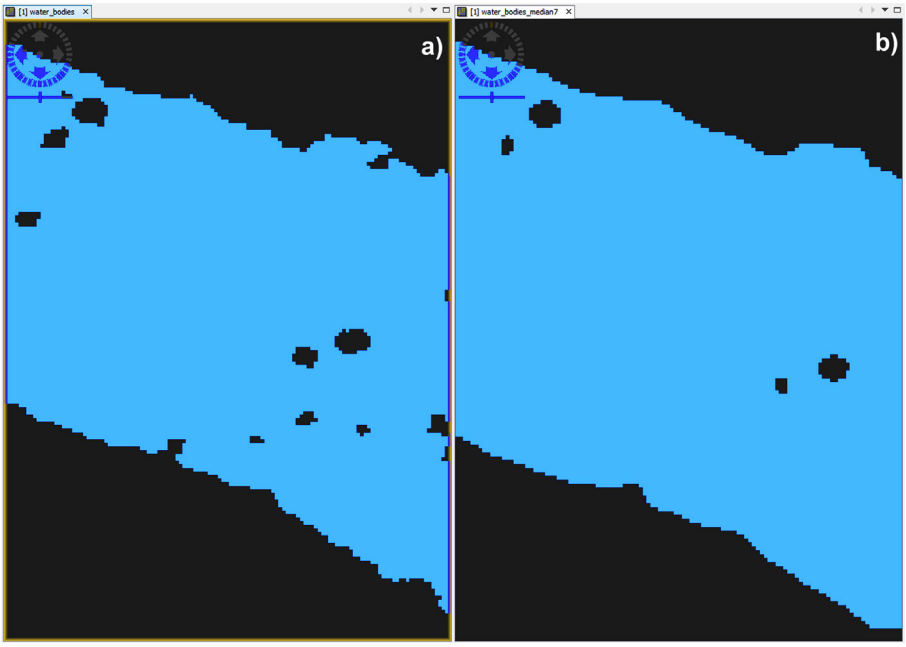

Figure 9. Generalization – Applying a low-bandwidth median filter with a convolution kernel of 7 x 7 pixels to result 8, smaller contrasting areas have been removed (small flooded and small dry within larger flooded) thus achieving partial geographic generalization.

The final result is georeferenced and can, as a thematic layer, overlap over a standard geographical background. In this paper, the result is translated into KML format (Keyhole Markup Language) and folded over an orthogonal projection in Google Maps (Figures 10, 11, and 12).

Results

The duration of the natural disaster in the Vrgorac region was monitored on four satellite images, during the passages of the Sentinel-1A satellite:

- October 30, 2020 around 04:50 GMT
- December 6, 2020 around 16:50 GMT
- December 12, 2020, around 04:50 GMT
- December 18, 2020, around 16:50 GMT.

October 30 image has not yet detected flooded areas, despite heavy rainfall, so it is not shown below. There are no lakes or larger bodies of water in that image, and in the event that we had them in a non-flooded area, we would have to monitor the difference between water bodies before and during the flooding.

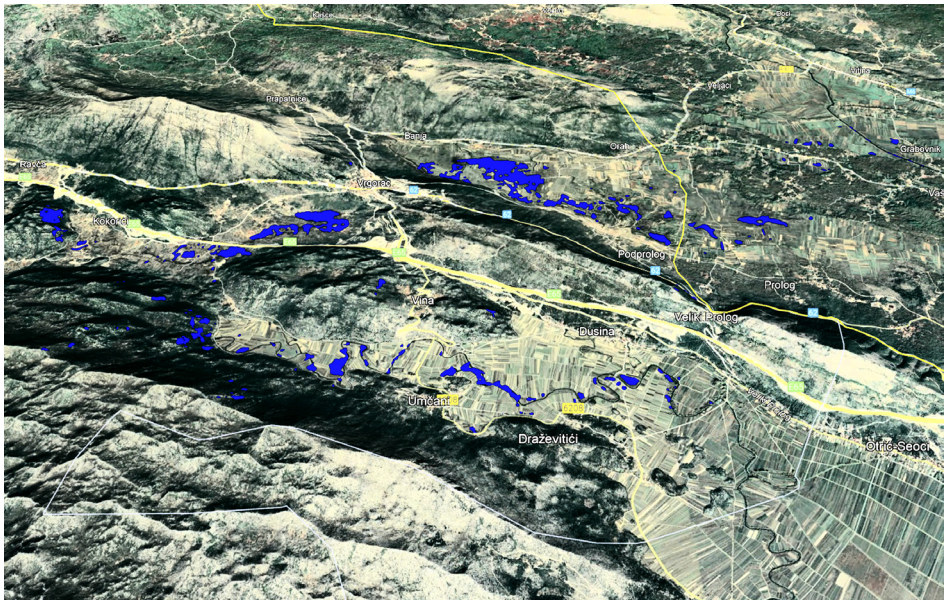

Figure 10. Beginning of the flood – Flooded areas detected on the Sentinel-1A satellite image on December 6, 2020, at around 5:50 pm local time, watercourses overflow and gradual flooding of lowland areas are observed.

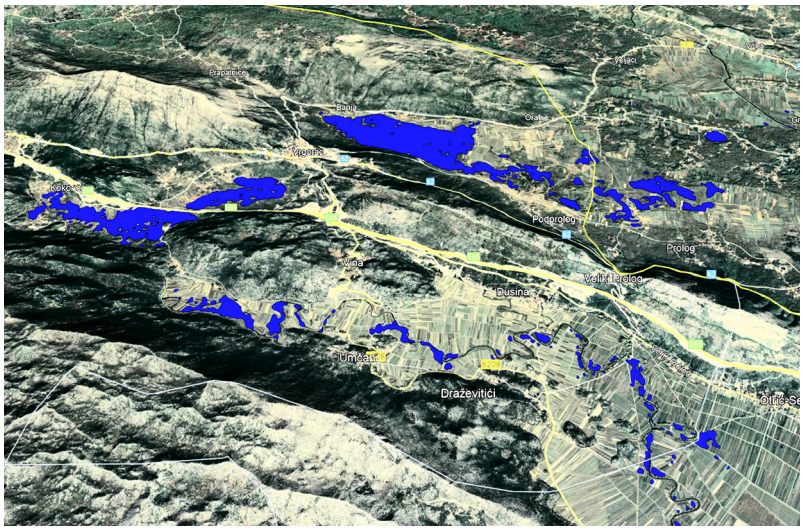

Figure 11. Flood peak – Flooded areas detected on the Sentinel-1A satellite image on December 12, 2020, around 05:50 local time, at the time of the flood peak.

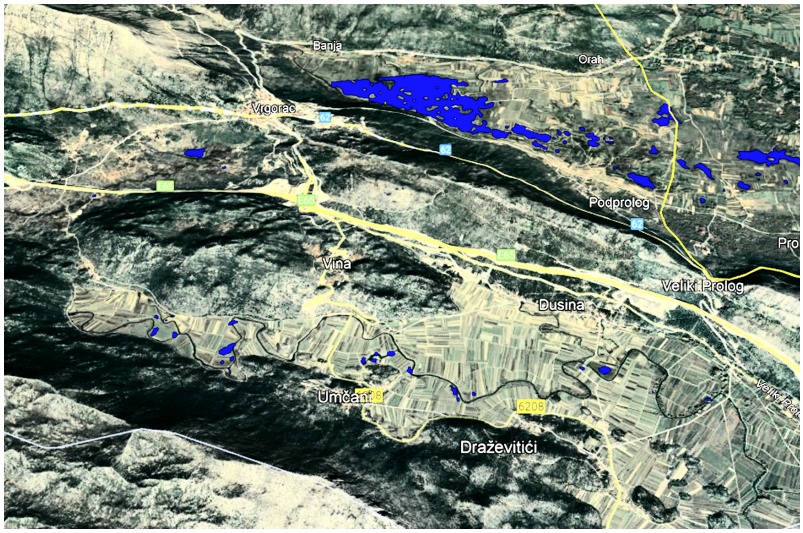

Figure 12. End of the flood – Flooded areas detected on the Sentinel-1A satellite image on December 18, 2020, around 5:50 pm local time, in the period when the water began to gradually recede.

Figures 10, 11, and 12 show the development of the situation during the natural disaster, the floods in the Vrgorac region, in November and December 2020. They are directly applicable to GEOINT support to military support operations in cases of natural and technical disasters. From them, it is possible to estimate the threat to people and property, to assess the passability of the terrain and the availability of road communications, and to determine meeting points for people and equipment during the operation. They can also be used to quickly assess damage and after action reports.

Conclusion

The application of image radar, specifically SAR sensors on the Sentinel-1 satellite pair, in polarimetric mode, for detection and monitoring of flooded surfaces has a number of advantages. The method itself is not numerically demanding and is quickly applied. On the operational side, the advantages of using Copernicus resources are openness and the possibility of support from the broad scientific and professional community. Copernicus satellite resources, on the other hand, offer limited operational capabilities due to relatively low time resolution, in this case once every six days. During natural disasters, especially floods, the situation on the ground changes rapidly and the necessary information should be obtained by satellite remote sensing several times a day. Commercial satellites, such as COSMO SkyMed and Radarsat, are expensive and the prices of their images reach thousands of euros. For example, the use of images from the COSMO SkyMed satellite, with a time resolution of 6 hours, in ScanSAR resolution of 30 x 30 m, during the observed period of natural disaster in the Vrgorac region, would amount to more than EUR 138,000 (e-GEOS, 2017).

The detection threshold method presented in this paper is optimal in terms of speed and requirement for computer resources (processor speed and memory space), and proved to be good even in highly developed karst orography, with isolated false positives on the descending terrain gradient "From the radar". The implementation of the method can be carried out independently of the available application for satellite image processing, and in this paper the Sentinel Applications Program, SNAP 8.0.7 was used.

Segmented water surfaces can be used as input parameters in hydrological and terrain models, thus significantly objectifying and automating the process of Rapid Environmental Assessment (REA) in the planning and implementation of military operations.

Recommendations

In cases of major natural and technical disasters, high-quality satellite imagery can be obtained without payment through the Charter on Space and Disasters (https://disasterscharter.org). Leading space agencies, bearing in mind the need to have all GEOINT information, make available satellite images and GIS data of affected areas, but only to state institutions in charge of crisis situations at the national level. At the time of writing, the Republic of Croatia has not yet signed the Charter and has designated an expert team to process and disseminate data received through the Charter. Given the fact that we live in an environment where natural and technical disasters are quite certain, it is necessary that we accede to the Charter at the national level as soon as possible. In parallel, it will be necessary to create a national team capable of retrieving and processing satellite images obtained from various sensors and producing thematic bases according to military quality standards and formats that can be delivered to existing C2 channels to field forces. Copernicus resources, which are an excellent resource for the education and training of this type of professionals, can play a major role in this. One such initiative could be implemented in less than a year.

Bibliography resources

Anusha, N., Bharathi, B. (2019) Flood detection and flood mapping using multi-temporal synthetic aperture radar and optical data, *The Egyptian Journal of Remote Sensing and Space Sciences, 23*, DOI: 10.1016/j.ejrs.2019.01.001, 207-219

e-GEOS (2017) e-GEOS Price List, BDS-COM-17-002, 52 pp.

Moriera, A., Prats-Iraola, P., Younis, M., Krieger, G., Hajnsek, I., Papathanassiou, P. (2013) A Tutorial on Synthetic Aperture Radar, I*EE Geoscience and Remote Sensing Magazine, March 2013*, DOI: 10.1109/MGRS.2013.2248301, 38 pp.

Mason, D. C., Dance, S. L., Cloke, H. L. (2021) Floodwater detection in urban areas using Sentinel-1 and WorldDEM data, *Journal of Applied Remote Sensing, Jul-Sep 2021, Vol 15(3)*, DOI: 10.1117/1.JRS.15.032003, 22 pp.

Rubel, O., Lukin, V., Rubel, A., Egiazarian K. (2019) NN-Based Prediction of Sentinel-1 SAR Image Filtering Efficiency, DOI:10.3390/geosciences9070290 , *Geosciences, vol. 9,no. 7*, 22 p.

Miranda, N. & Meadows, P. J. (2015) Radiometric Calibration of S-1 Level-1 Products Generated by the S-1 IPF, *ESA Technical Note SA-EOPG-CSCOP-TN-0002*, European Space Agency, 13 pp.

Veci, L. (2016) Sentinel-1 Toolbox – Polarimetric Tutorial, ESA & Array Systems Computing Inc., 29 pp

Viher, M., Žiža, I., Radun, B., Tomljenović, I., Čvrljak, M., Kušan, V., Vuković, V., Knežević, L. (2021) GEOINT in Natural and Technical Disasters, *Proceedings of 1st Croatian Conference on Earthquake Engineering, 1CroCEE, Zagreb, Croatia - March 22nd to 24nd*, 397-403

Yamaguchi, Y. (2020) Polarimetric SAR Imaging, ISBN: 978-0-367-47831-5, Taylor & Francis Group, 350 pp.

Župan, R., Frangeš, S., Vinković, A. (2019a) Normalized water index for mapping a flood, *ISEM - The International Society for Ecological Modelling Global Conference 2019*, 1.-5.10.2019., Salzburg, Austrija

Župan, R., Frangeš, S., Vinković, A. (2019b) What Method to Use for Fast Mapping of Flooded Area?, *15th International conference Geoinformation and Cartography - Program and Abstracts*, Lapaine, M. (ed.). Zagreb: Croatian Cartographic Society, 2019. p. 39-39

Župan, R., Frangeš, S., Molak-Župan, Ž., Vinković, A. (2019c) Flood Analysis Using Sentinel Images and Mapping, *World Multidisciplinary Earth Sciences Symposium (WMESS 2019) - Abstract collection book* / Ashton, A. – P. (ur.). Praha: IOP Publishing Ltd, 2019. p. 293-293

O autoru

Colonel, Assistant Professor MLADEN VIHER, PhD (mladen.viher@morh.hr) received his PhD in physics and geophysics from the Faculty of Science, University of Zagreb, in 2011. At the time of writing this paper, he is the head of the University's Department of Technical Development and Research at the Janko Bobetko Centre for Defence and Strategic Studies at the Dr. Franjo Tuđman Croatian Defence Academy. From 2015 to 2020, he was the national representative in the NATO Science and Technology Organization Panel for Sensors and Electronic Technologies, and since 2020 he has been the National Director for Research and Technology in the Directorate of the European Defence Agency for Research, Technology and Innovation (EDA-RTI). He has been engaged in research in the fields of remote sensing, propagation of electromagnetic waves in the atmosphere and the application of data science in the management of scientific research for defence and security purposes.